A Methane−Water Model for Coarse-Grained Simulations of Solutions and Clathrate Hydrates

Liam C. Jacobson and Valeria Molinero*

Department of Chemistry, University of Utah, 315 South 1400 East, Salt Lake City, Utah 84112-0850

Received: February 12, 2010; Revised Manuscript Received: April 19, 2010

Methane is the prototypic hydrophobic molecule; it has an extremely low solubility in liquid water that leads to phase segregation. On the other hand, at moderate pressures and room temperature, water and methane form hydrate clathrate crystals with a methane to water ratio up to a 1000 times higher than the saturated aqueous phase. This apparent dichotomy points to a subtle balance between the strong water−water hydrogen bonding, responsible for the hydrophobic effect, and water−methane attraction. Capturing these nuances with molecular models requires an appropriate balance of intermolecular interactions. Here we present such a coarse-grained molecular model of water and methane that represents each molecule by a single particle interacting through very short-range interaction potentials. The model is based on the monatomic model of water mW [Molinero, V.; Moore, E. B. *J. Phys. Chem. B* **2009**, *113*, 4008] and is between 2 and 3 orders of magnitude more computationally efficient than atomistic models with Ewald sums. The coarse-grained model of this study reproduces the solubility and hydration number of methane in liquid water, the surface tension of the water−methane interface and the equilibrium melting temperature of methane hydrate clathrates with structures sI and sII. To the best of our knowledge this is the first force-field, atomistic or coarse-grained, that reproduces these range of properties of liquid and solid phases of water and methane, making it an efficient and accurate model for the study of the mechanisms of nucleation and growth of clathrates. We expect that the results of this work will also be useful for the modeling of the hydrophobic assembly in aqueous solutions and the development of coarse-grained models of biomolecules with explicit solvation.

I. Introduction

Methane and water have extremely low mutual solubility and segregate in solution. Nevertheless, water and methane form hydrate clathrate crystals with a methane to water ratio up to a 1000 times higher than the saturated aqueous phase. Methane clathrates are nonstoichiometric crystals of water and methane, in which water forms a fully hydrogen-bonded network of polyhedral cages that contain the methane guest.[1] Natural gas hydrates normally form at high pressures and occur naturally on the ocean floor and in the permafrost.[2] Gas hydrates have gained much attention recently due to their promise as an abundant alternative energy source[3] as well as a possible vehicle for carbon sequestration.[4,5] Methane hydrates are of particular interest because, according to some estimates there is more energy contained in methane clathrate deposits than there is energy from all other conventional fossil fuel sources combined.[2] On the other hand, the occurrence of clathrate hydrates in natural gas pipelines is of great concern to the petroleum industry, because as they form in the high-pressure pipelines, they create clogs that stop the flow of gas and disrupt production, increase costs, and present a safety hazard.[2,6] Accurate modeling of the microscopic mechanisms of nucleation, growth, and decomposition of methane clathrates is important for creating clathrate inhibitors as well as devising methods to extract methane from clathrate reserves on an industrial scale.

Under pressure, methane clathrates are stable at ambient temperatures. The dissociation (also called melting) temperature of methane clathrate at 100 atm, for example, is 286.2 K, about 14 K higher than that of hexagonal ice under the same pressure. The hydrogen-bonded water network that forms the clathrate frame accounts for most of the stability of these crystals. In two independent simulation studies, using different models and simulation methodologies, Jacobson et al.[7] and Conde et al.[8] predicted that the guest-free clathrate crystal with the sII structure is a stable phase of water under extension. Our study indicates that at room temperature guest-free water clathrates are metastable with respect to ice Ih and would have a melting temperature of ∼250 K. An extrapolation of the results from ref 8 suggests an even lower value. Thus, while the water−methane attraction is weak, it is key for the formation and stabilization of methane hydrate.

Clathrate hydrates occur predominantly in two cubic structures known as sI and sII. The sI crystal is the most stable methane hydrate. Nevertheless, sI and sII crystals form together during the initial stages of growth of methane hydrate.[9,10] Using the CSM-Gem program by Sloan and co-workers,[11] which calculates multiphase equilibrium using a Gibbs free energy minimization algorithm and reproduces the experimental phase diagram of methane clathrate,[11] we find that the melting temperatures T_m of sI and sII methane hydrates differ by just 1.5 K at 100 atm. We hypothesize that the small difference in T_m (and thus in free energy) between the two crystals is responsible for the occurrence of the stable sI and metastable sII structures in the first stages of crystallization observed both in experimental[9,10] and in computational[12,13] studies. The ability of molecular simulations in reproducing and explaining the polymorphism in the growth of methane clathrates would probably depend on the accuracy of the molecular models in reproducing the closeness of the melting temperatures.

* Corresponding author. E-mail: Valeria.Molinero@utah.edu.

10.1021/jp1013576
Published on Web 05/12/2010

Atomistic simulations of methane−water systems have given valuable insight on the thermodynamic stability,[14,15] growth[16,17] and decomposition,[18,19] anomalous thermal properties,[20,21] and nucleation[12,22] of methane hydrates, as well as on hydrophobic hydration.[23−28] Atomistic models of water−methane systems are normally derived from water and methane potentials that were parametrized and validated for properties of the pure substances. The water−methane interaction parameters are then obtained using combination rules and are typically not validated with experimental thermodynamic data such as melting temperature, enthalpy of dissociation, and solubility. Docherty et al. recently demonstrated that the use of combination rules for water−methane interactions is inadequate to reproduce the solubility of methane, even when the most accurate water and methane potentials are employed.[25]

The models of water used in the simulation of clathrates predict widely different melting temperatures for ice. Of the atomistic models, only TIP4P/ice correctly predicts the experimental T_m of hexagonal ice Ih;[29] widely used models such as SPC, SPC/E, TIP3P, and TIP5P incorrectly predict that ice II and not Ih is the most stable ice crystal at room pressure.[30] It would be expected that a similar variability be observed in the melting temperatures predicted for methane hydrates. Although it is crucial to know the melting temperatures of sI and sII methane clathrate crystals for the modeling and interpretation of the mechanisms of clathrate formation, scarce thermodynamic data are available for the molecular models used for clathrate modeling. The T_m of sI methane hydrate is known for just a couple of atomistic force-fields,[31,32] and (to the best of our knowledge) the T_m of its sII polymorph has never been computed with molecular simulations.

In this work we present the parametrization and validation of a methane−water model that reproduces the experimental hydration number and solubility of methane in water and the melting temperatures of sI and sII methane hydrates. Solubility and melting temperatures are the two most important thermodynamic properties that control the crystallization of clathrates. The hydration number in solution should play a role in the magnitude of the barrier for clathrate nucleation. Different from other models available for simulations of clathrates and aqueous methane, here we present a coarse-grained molecular model. We develop a united-atom methane model and combine it with the monatomic model of water mW, which represents the water molecule by a single particle interacting through very short-ranged potentials.[33] Although mW water does not have hydrogen atoms or even electrostatic interactions, it reproduces the structure of the liquid and crystal phases of water through the use of three-body terms in the potential that encourage "hydrogen-bonded" tetrahedral configurations of the molecules. The mW model reproduces the temperature of melting, enthalpies of vaporization, melting and sublimation of water, and the liquid−vapor surface tension with precision equal or higher than the most popular atomistic water models.[33] It also reproduces the experimental radial and angular structure of liquid water and low-density amorphous ice, as well as the structure, nucleation, and growth of ice in bulk and in confinement.[7,33−36] The monatomic model correctly produces the thermodynamic and dynamic anomalies of water (increase in heat capacity on cooling, density maximum, increase of diffusivity on compression) as well as the transformation of liquid water to low-density amorphous ice and the increase in correlation length that accompanies the structural transformation of water on cooling at room pressure.[33,36] Most important for this work, mW describes the thermodynamics of guest-free clathrates, the growth of empty and filled hydrates, and the nucleation of hydrates with hydrophobic guest molecules.[7,13,37]

The main advantage of a coarse-grained model is its computational efficiency: simulations with the mW model are 180 times faster than with atomistic water models with Ewald sums.[33] An accurate and well-characterized coarse-grained model of methane and water would permit the study of the mechanisms of nucleation and growth of methane clathrates under various thermodynamic conditions with knowledge of the crystallization driving force.

Although there are benefits to using a coarse-grained water model, there are challenges associated with it as well. How well can the hydration structure around methane and the structure of the water−methane interface be reproduced using a potential that does not have atomistic resolution? Is it possible to simultaneously reproduce the solubility in liquid water and the melting temperatures of the sI and sII hydrates? Our goal in this study is to develop coarse-grained methane−methane and water−methane potentials that, in conjunction with the mW model for water, would reproduce the thermodynamics of aqueous methane and methane hydrate. We outline a strategy to parametrize the water−methane interactions and evaluate the parametrization by comparing the results of simulations with experimental values of melting temperature and enthalpy of dissociation of the hydrate, and the hydrophobic solvation of methane in water. We discuss the implications of removing degrees of freedom on the thermodynamics of dissociation of the hydrates when going from a model with atomistic resolution to a coarse-grained one.

The paper is organized as follows: In section II we describe the simulation methodology and introduce the systems modeled in this study. Section III presents the force fields: we describe the mW model, introduce the functional form of the potential for methane−methane and methane−water interactions, the parametrization of the former, and the strategy for the parametrization of the latter. The data necessary for the parametrization and validation of the water−methane interaction are presented in sections IV and V: section IV focus on the thermodynamics of clathrate formation and section V on the structure and thermodynamics of methane−water solutions. Section VI presents a summary and the most important conclusions of this work.

II. Simulation Methods

A. Simulations. Molecular dynamics (MD) simulations were performed using LAMMPS, a massively parallel MD software by Plimpton et al.[38] The absence of fast molecular rotational modes in the coarse-grained models allows for the integration of the equations of motion (velocity Verlet algorithm) with a time step of 10 fs.[33] Periodic boundary conditions were used for all systems. Except when otherwise indicated, the simulations were done in the *NpT* ensemble, with the temperature and pressure regulated by a Nose−Hoover thermostat and barostat with damping constants 5 and 25 ps, respectively. For systems with coexisting liquid and crystal phases, the three cell dimensions were allowed to dilate and contract independently.

B. Systems. ***Fluid Simulations.*** Liquid mixtures consisting of 5 methane and 507 water molecules were evolved for 800 ns at 300 K and 100 atm to gather data for the calculation of the radial distribution function between methane and water. Methane solubility and density profiles were determined from 100 ns simulations of two-phase methane−water systems containing 16 000 molecules (14 851 water molecules and 1149 methane molecules) with cell dimensions approximately 230

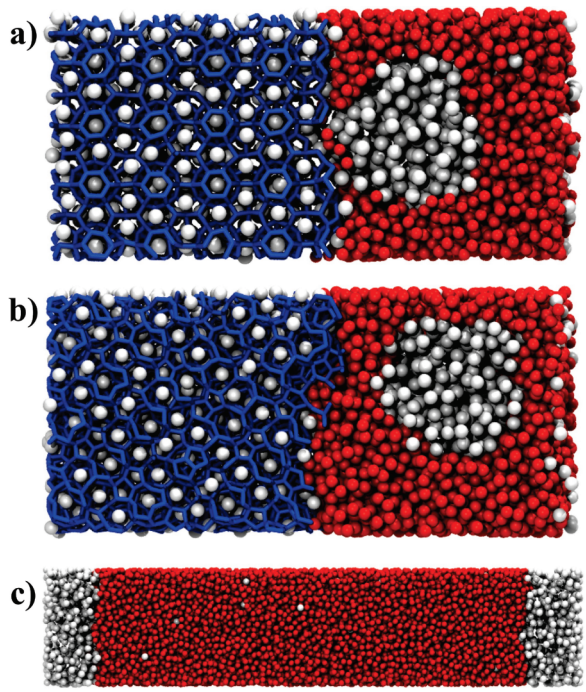

Figure 1. Simulation cells used in the phase-coexistence simulations: (a) phase coexistence of sI methane clathrate with the water-rich and methane-rich liquids; (b) phase coexistence of sII methane clathrate with the water-rich and methane-rich liquids; (c) phase coexistence of the water-rich and methane-rich liquid. Methane molecules depicted as white balls, water molecules connected by blue sticks when they are part of the clathrate cages and displayed as red balls otherwise.

× 50 × 50 Å. Fluid methane simulations were performed with systems containing 1728 coarse-grained methane particles and liquid water simulations with 9936 coarse-grained water particles. The pure liquids were equilibrated over 10 ns at the T and p conditions indicated in the text.

Crystal Simulations. Crystal structures of methane clathrate hydrates were used for the calculations of the enthalpy and the mapping of the regions of stability of each structure. The sI crystals consisted of 4 × 4 × 4 unit cells containing 2944 water molecules and 512 or 384 guest molecules. The sII crystals consisted of 3 × 3 × 3 unit cells containing 3672 water molecules and 648 or 216 guest molecules. The two methane contents for each structure correspond to all polyhedral cages occupied by methane and only the large cages occupied, respectively. The enthalpy of each crystal was averaged over 100 ps simulations for each point of the stability map as well as for the calculation of the enthalpy of dissociation of the clathrates.

Three-Phase Liquid-Crystal Coexistence Simulations. The systems used for melting point determinations were derived from a hydrate lattice (8 × 4 × 4 unit cells consisting of 5888 water molecules and 1024 guest molecules for sI and 6 × 3 × 3 unit cells consisting of 7344 water molecules and 1296 guest molecules for sII). Half of the crystal cell was melted and the liquid was first equilibrated for 10 ns to allow for the phase segregation of aqueous and methane phases. These three-phase coexistence systems are shown in the top two panels of Figure 1. The three-phase systems were evolved at various temperatures at $p = 100$ atm to allow the determination of the melting temperature through the direct coexistence method described in section IV. Individual simulations for temperatures close to the melting point were carried for as long as 650 ns.

III. Coarse-Grained Models and Force Fields

A. Water Model. The monatomic model of water (mW) represents a water molecule by a single particle that interacts through very short-ranged potentials.[33] The interaction in mW water has the form of the Stillinger−Weber potential:[39]

$$E = \sum_i \sum_{j>i} \phi_2(r_{ij}) + \sum_i \sum_{j\neq i} \sum_{k>j} \phi_3(r_{ij},r_{ik},\theta_{ijk})$$
$$\phi_2(r_{ij}) = A\varepsilon\left[B\left(\frac{\sigma}{r_{ij}}\right)^4 - 1\right]\exp\left(\frac{\sigma}{r_{ij} - a\sigma}\right)$$
$$\phi_3(r_{ij},r_{ik},\theta_{ijk}) = \lambda\varepsilon[\cos\theta_{ijk} - \cos\theta_0]^2 \exp\left(\frac{\gamma\sigma}{r_{ij} - a\sigma}\right)\exp\left(\frac{\gamma\sigma}{r_{ij} - a\sigma}\right) \quad (1)$$

where r_{ij} is the distance between particles i and j and θ_{ijk} is the angle subtended by the vectors between the positions of the $i-j$ and $i-k$ pairs of particles. The constants $A = 7.049\,556\,277$, $B = 0.602\,224\,558\,4$, $\gamma = 1.2$, $a = 1.8$, and $\theta_o = 109.5°$ are the same for mW water and the original SW silicon potential.[39] The three-body terms encourage "hydrogen-bonded" configurations between mW waters by imposing a penalty to configurations with water−water−water angles that depart from the tetrahedral value, $\theta_o = 109.5°$. The value of the parameter λ determines the strength of the tetrahedral interactions. All intermolecular forces vanish at a cutoff distance $r_c = a\sigma = 1.8\sigma$.

The interaction strength $\varepsilon_w = 6.189$ kcal/mol, characteristic distance $\sigma_w = 2.3925$ Å, and the tetrahedral parameter $\lambda_w = 23.15$ of the monatomic mW were optimized in ref 33 to reproduce the experimental enthalpy of vaporization and density of liquid water at 298 K and 1 atm, and the melting temperature of hexagonal ice.

B. Methane Model. The level of coarsening of the methane model of this study is the same as the OPLS united-atom (OPLS-UA) methane model:[40] a methane molecule is represented by a single particle. The OPLS-UA model uses the Lennard-Jones 12-6 potential to describe methane−methane interactions, and it reproduces the experimental heat of vaporization, density, and vapor−liquid coexistence curve of methane.[40−42] The interactions in OPLS-UA methane extend at distances considerably longer than in mW water. The combination of coarse-grained potentials with different length scales and softness produces unphysical results.[43] Here we use the two-body term of the Stillinger−Weber (SW) potential (ϕ_2 in eq 1) to describe methane−methane interactions. We set $\lambda = 0$ for methane triplets because, different from water, methane interactions are well represented by isotropic potentials. The values of A, B, and a in eq 1 are the same as listed above for mW. In what follows, we use the acronym M_{SW} to designate the coarse-grained methane model with the short-ranged SW interactions.

We adjusted the characteristic size σ_m and interaction strength ε_m between methane particles to reproduce the volume and enthalpy of vaporization, ΔH_{vap}, of methane at its boiling point at $p = 1$ atm and $T = 111.66$ K. ΔH_{vap} of the M_{SW} model was calculated as the difference in the molar enthalpy of the gas and the liquid at these conditions. The ensemble average of the enthalpy, $\langle H\rangle = \langle E + pV\rangle$ of the liquid was determined from NpT simulations of 1728 methane particles for 10 ns. The methane gas was assumed to be ideal: $H_{gas} = 1.5\,RT + pV_{gas} = 2.5\,RT$. Table 1 lists σ_m and ε_m for methane−methane interactions in M_{SW}. The model reproduces the experimental enthalpy of vaporization (1.95 ± 0.02 kcal/mol compared to 1.96 kcal/mol[40]) and density (0.424 ± 0.003 g/mL compared to 0.424 g/mL[40]).

TABLE 1: Interaction Parameters for the Coarse-Grained Model

	ε (kcal/mol)	σ (Å)	λ
water[a]	6.189	2.3925	23.15
methane	0.340	4.08	0
water−methane	0.180	4.00	0

[a] Reference 33. Interactions potential described by eq 1 with the other constants same as for mW.

TABLE 2: Density of Fluid Methane at $T = 300$ K

	ρ_{Exp}[a] (g/mL)	$\rho_{OPLS\text{-}UA}$ (g/mL)	ρ_{Msw} (g/mL)	ρ_{Msw}/ρ_{Exp}
1 atm	6.4×10^{-4}	6.6×10^{-4}	6.5×10^{-4}	1.01
50 atm	0.035	0.035	0.039	1.11
100 atm	0.075	0.075	0.10	1.33

[a] The experimental density of methane was computed using the equation of state from ref 44.

TABLE 3: Enthalpy of Fluid Methane at 300 K

	$H^{OPLS\text{-}UA}$ (kcal/mol)	H^{Msw} (kcal/mol)	$H^{Msw}/H^{OPLS\text{-}UA}$
1 atm	1.49	1.48	0.99
50 atm	1.31	1.20	0.92
100 atm	1.13	0.82	0.73

Table 2 shows the density of methane at 300 K as a function of pressure in experiments and in our simulations with the OPLS-UA and M_{SW} models. OPLS-UA methane reproduces the equation of state of methane in the range of pressures presented in Table 1.[44] The M_{SW} model reproduces the experimental density at 1 atm, but the agreement degrades at high pressures because the softer repulsive region of M_{SW} methane makes it more compressible than OPLS-UA methane. In terms of its impact on the dissociation equilibrium of methane clathrates, the density of methane is less important than its enthalpy. Table 3 shows the molar enthalpy of methane as a function of pressure for the OPLS-UA and M_{SW} models at $T = 300$ K. As observed for the density, the agreement is better at low pressures. M_{SW} underestimates the enthalpy at high pressures, probably due to the extremely short-ranged nature of the potential. A pressure of 1 atm was chosen for the parametrization of M_{SW} methane because this is the pressure for which mW water was parametrized. It is possible to parametrize M_{SW} to reproduce the experimental high-pressure behavior of methane, but we consider it unnecessary because water−water and water−methane interactions dominate the thermodynamics of clathrate formation: the error in the enthalpy of methane at 300 K and 100 atm is just 2.4% of the experimental enthalpy of dissociation of sI methane hydrate, $\Delta H_d = 13.01$ kcal/mol, under the same conditions.[45]

C. Methane−Water Interactions. Water does not form hydrogen bonds with methane; thus we set set $\lambda = 0$ for triplets that contain water and methane. The water−methane potential is described by the two-body term of eq 1 with A, B, and a identical to those of mW, as we did for the methane−methane potential. In what follows we explain the strategy we adopt in this study to determine the two remaining parameters: the characteristic distance σ_{wm} and strength of the attraction ε_{wm} of the water−methane potential.

In atomistic simulations, the cross-parameters σ_{wm} and ε_{wm} are typically derived using Lorentz−Berthelot combination rules of the parameters of the water−water and methane−methane interactions. Vega and co-workers have shown that such combination rules for the water−methane interaction in rigid water models are unable to reproduce the experimental value of the solubility of methane in water.[25] They suggest that the cause is the lack of polarizability in the rigid water models that they compensate by scaling up 7% the attraction strength ε between water and methane in a nonpolarizable model. Most of the water−water attraction in atomistic models results from electrostatic interactions and ε_{ww} is small, around 0.15 kcal/mol. In mW water, on the other hand, there are no electrostatic interactions and ε_{ww} is about 40 times larger. Use of combination rules would result in a very attractive water−methane potential, inconsistent with the known hydrophobicity of methane. Combination rules are not a good starting point to search for the optimum ε_{wm} in the coarse-grained model.

To optimize ε_{wm} and σ_{wm} of the coarse-grained model, we produce a set of candidate solute−water parameters for which we compute (i) the melting temperature T_m of the clathrates with structures sI and sII, (ii) the corresponding enthalpy of dissociation ΔH_d of the sI methane clathrate, (iii) the solubility x_m of methane in water, and (iv) the hydration number n_w of methane in water at infinite dilution. The best values of ε_{wm} and σ_{wm} are then determined by comparison of the predictions of the simulations with the experiments.

As a guide for the parametrization, we map out the regions of stability for clathrates with guest methane molecules of different structures and stoichiometry in the [σ_{wm}; ε_{wm}] parameter space. The stable crystal for each value of [σ_{wm}; ε_{wm}] is approximated as that with the lowest enthalpy of formation. A more rigorous calculation of the stabilities based on free energies is unnecessary because the map is used only as a guide for the parametrization. Using the fully occupied sII crystal as reference, we computed the difference in enthalpy for the following processes (subscripts indicate partial crystal occupancy):

$$
\begin{aligned}
&23\text{sII} \leftrightarrow 68\text{sI} + 8\text{CH}_4\\
&\left(1\text{H}_2\text{O} + \frac{3}{17}\text{CH}_4\right) \leftrightarrow \left(1\text{H}_2\text{O} + \frac{4}{23}\text{CH}_4\right) + \frac{1}{391}\text{CH}_4\\
&23\text{sII} \leftrightarrow 68\text{sI}_{(\text{empty dodecahedra})} + 144\text{CH}_4\\
&\left(1\text{H}_2\text{O} + \frac{3}{17}\text{CH}_4\right) \leftrightarrow \left(1\text{H}_2\text{O} + \frac{3}{23}\text{CH}_4\right) + \frac{18}{391}\text{CH}_4\\
&23\text{sII} \leftrightarrow 23\text{sII}_{(\text{empty dodecahedra})} + 368\text{CH}_4\\
&\left(1\text{H}_2\text{O} + \frac{3}{17}\text{CH}_4\right) \leftrightarrow \left(1\text{H}_2\text{O} + \frac{1}{17}\text{CH}_4\right) + \frac{2}{17}\text{CH}_4
\end{aligned}
\tag{2}
$$

The enthalpies of sI and sII clathrates at 100 atm and 300 K with (i) all cages occupied by methane and (ii) only the large cages filled were calculated for 3 Å < σ_{wm} < 5 Å (evaluated every 0.1 Å) and 0.1 < ε_{wm} < 0.4 kcal/mol (evaluated every 0.05 kcal/mol). The last element of the calculations, the enthalpy of methane under the same conditions, was taken from Table 3.

The resulting "stability map" as a function of σ_{wm} and ε_{wm} is shown in Figure 2. The "stability region" of each structure encompasses the values of water−methane parameters for which that crystal has the lowest enthalpy of formation. The order of the structures in terms of σ_{wm} is representative of the trend in guest size determined in experiments.[1] The smallest guest molecules favor the sII structure (also the most stable in the absence of guests[7,8]) but larger guest molecules that struggle to fit in the small dodecahedral cages stabilize the sI crystal because it has a higher ratio of large to small cages. Only the sII structure has cages large enough to accommodate the largest guest molecules. As σ_{wm} and ε_{wm} become smaller, the sII structure is favored.

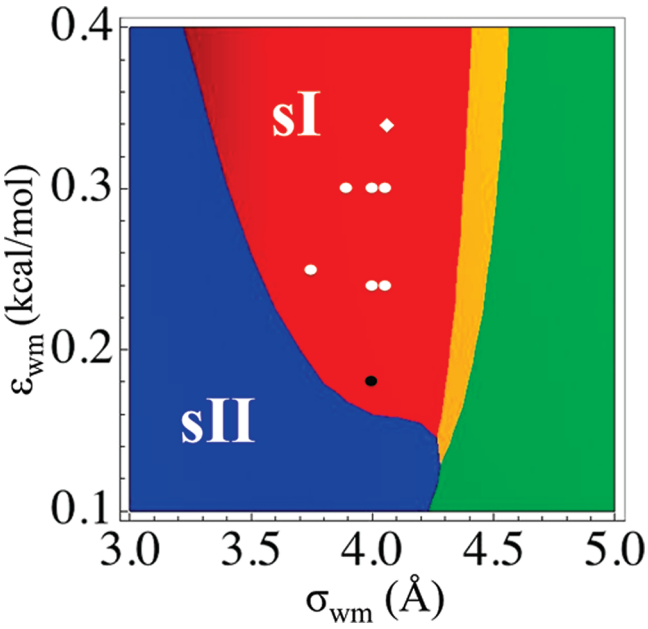

Figure 2. Regions of stability of sI and sII clathrates as a function of the water−methane interaction parameters, σ_{mw} and ε_{mw}. The colored areas indicate the regions where a clathrate structure has the lowest enthalpy of formation: blue corresponds to the sII structure with all cages occupied, red to the fully occupied sI crystal, yellow to the sI structure with occupied large cages and empty dodecahedral cages, and green to the sII structure with filled large cages and empty dodecahedral cages. The diamond indicates the parameters used for the methane−methane interactions. The circles represent the set of [σ_{wm}; ε_{wm}] parameters evaluated in this study (results listed in Table 4). The black circle indicates the parameters that best reproduce the T_m and solubility of methane, $\sigma_{wm} = 4.0$ Å and $\varepsilon_{wm} = 0.18$ kcal/mol.

Once the regions of stability were mapped, we focused our search on the region of Figure 2 where the sI methane hydrate with small and large cages occupied is the most stable crystal, as found in the experiments.[2] Sections IV and V present the analysis of the thermodynamics and structure of solutions and clathrates for which the water−guest interaction parameters lie within this region of the [σ_{wm}; ε_{wm}] space. The best methane−water parameters that result from a comparative analysis of the melting temperatures, methane solubility, and hydration number are listed in Table 1.

Molecular dynamics simulations of water corresponding to a given amount of time (e.g., 100 ns) take 180 times less computing time with mW than with atomistic water models using Ewald sums.[33] The increase in efficiency is due to the larger time steps, the decrease in the number of particles, and the extremely short-range of the interaction potentials. We refer the readers to refs 33 and 43 for details on the benchmarking of mW against the atomistic SPC/E water model and the scaling of the computing cost with the number of particles (better than for Ewald sums and slightly less favorable than for particle−particle−particle mesh Ewald). Calculations of methane−methane and methane−water interactions are faster than among water molecules, because they do not involve the more expensive calculations of the three-body forces in the potential (to this end, we modified the standard version of the Stillinger−Weber potential in LAMMPS to avoid the three-body loops when $\lambda = 0$). We benchmarked the simulation times for liquid systems composed of 6912 particles of (i) model water, (ii) M_{SW} methane, and (iii) half methane and half water, and found that pure M_{SW} simulations are about 13 times faster than the pure mW, and a 1:1 mixture of model water and M_{SW} methane is twice as fast as pure model water. On this basis, we conclude that, depending on the ratio of water and methane, this coarse-grained model speeds up the simulations by 2−3 orders of magnitude compared to the atomistic ones.

IV. Thermodynamic Stability of sI and sII Methane Clathrates

A. Melting Temperatures of sI and sII Methane Hydrates.

Experiments indicate that the stable methane hydrate has the sI structure.[2] Nevertheless, several studies have shown that sII also forms in the initial stages of methane clathrate crystallization,[9,10] suggesting that the stabilities of sI and sII methane hydrates are similar. We computed the melting temperatures of these two crystals using the CSMGem program by Sloan and co-workers.[11] At $p = 100$ atm, the predicted T_m's for methane hydrate are 286.2 K for the sI structure and 284.7 K for the sII structure. The T_m for the most stable methane clathrate structure (sI) has been computed for very few force fields: TIP4P water and OPLS-AA methane predict a T_m of sI between 287 and 302 K at $p = 400$ atm[31] and the COS/G2 water model and five-site methane produce $T_m = 268 \pm 3$ K at $p = 67$ atm.[32] The melting temperature of the sII methane clathrate has not been reported for any force field.

In the melting (dissociation) of clathrates, three phases coexist in equilibrium: liquid water saturated with methane, fluid methane saturated with water, and the clathrate crystal. The melting temperatures (T_m) of the clathrates were determined using the method of direct coexistence.[46,47] The two upper panels of Figure 1 show snapshots of the three-phase systems used to determine T_m for the sI and sII clathrate crystals. This method involves performing simulations at constant pressure at a series of temperatures T for a system in which a crystal and the fluid phases are in direct coexistence. T_m was evaluated by determining at which temperature there was no net growth or decomposition of the clathrate phase. De Pablo and co-workers have used this method to determine the melting temperature of sI methane hydrate.[31] The fluid methane phase in our coexistence simulations is a cylinder (see Figure 1) because this is the shape that minimizes the area for the amount of methane in the cell. We show in section VA below that the solubility of methane in water (i.e., its chemical potential) with the cylinder and a slab of methane are indistinguishable. Thus, the melting temperatures determined in this study would be the same if measured with a slab configuration.

We determined the T_m of sI and sII structures at $p = 100$ atm for candidate water−methane parameters, [σ_{wm}; ε_{wm}], located in the region of the parameter space where the fully filled sI structure has the lowest enthalpy of formation (Figure 2). A pressure of 100 atm was selected because it is well within the hydrate-forming region of the methane hydrate phase diagram. Table 4 presents the T_m for a range of water−methane parameters. The error bar measures the temperature gap in which no net growth or dissolution could be observed. We note that within a few degrees of the melting temperature, simulations as long as 650 ns were needed to establish whether the system evolved toward the crystal or the liquid state, and in some cases there was no evolution toward crystal or liquid phase even in this time scale. The length of the simulations needed to produce a phase change close to the melting temperature grows increasingly longer as the water−methane interaction strength ε_{wm} decreases.

For all the [σ_{wm}; ε_{wm}] sets, we find that the T_m of sI is higher than, or equal within the error bar to, T_m of sII, consistent with the prediction of Figure 2. The difference between the two

TABLE 4: Thermodynamic and Structural Properties of Methane Clathrates and Aqueous Solutions as a Function of the Water−Methane Interaction Parameters

		methane−water interaction parameters [σ (Å); ε (kcal/mol)]						
property	experiment	[4.0; 0.18]	[4.05; 0.24]	[4.0; 0.24]	[4.0; 0.3]	[4.05; 0.3]	[3.90; 0.3]	[3.75; 0.25]
T_m sI	286.2[a]	285 ± 4	302.5 ± 1	308 ± 2	329 ± 1	323 ± 1	338 ± 2	333 ± 1
T_m sII	284.7[a]	286 ± 1	301 ± 1	304 ± 2	321 ± 1	318 ± 2	333 ± 2	329 ± 1
ΔH_d^{sI}	13.01 ± 0.35[b]	9.27	10.3	10.4	11.6	11.4	12.0	11.2
ΔS_d^{sI}	45	33	34	34	35	35	36	34
solubility	0.002325[c]	0.0022	0.0038	0.0049	0.015	0.013	0.018	0.012
hydration	20,[d] 19 ± 1[e]	19.3	19.7	19.7	21.8	21.7	20.9	18.9

[a] Calculated in the CSMGem software program,[11] [b] Reference 45. [c] Reference 48. [d] Reference 52. [e] Reference 51. Units: melting temperature T_m in K, solubility in methane molar fraction, enthalpy of dissociation ΔH_d in kcal/mol of methane, and entropy of dissociation ΔS_d in (cal/K)/mol of methane). ΔH_d and ΔS_d computed at $T = 300$ K and $p = 100$ atm, solubility at 313 K and 178 atm.

melting temperatures for the sI and sII crystals (ΔT_m) ranged from -1 ± 5 to 8 ± 2 K. The actual values of T_m increase with the strength of water−methane attraction ε_{wm} and decrease with increasing characteristic size σ_{wm}. The best agreement with the experiment is obtained for $\sigma_{wm} = 4.0$ Å and $\varepsilon_{wm} = 0.18$ kcal/mol, which predict $T_m = 285 \pm 4$ K for sI and 286 ± 1 for sII. The T_m for [4.0 Å; 0.18 kcal/mol] agree with the experiment within the precision of the simulations. The ΔT_m is -1 ± 5 K; thus, although it agrees with the 1.5 K predicted with the CSMGem program, the simulations cannot attain the level of precision required to distinguish two melting temperatures that are so close, even using the very long simulations of this study.

B. Enthalpy and Entropy of Dissociation of Methane Hydrate. If the methane and water liquids in equilibrium with methane hydrate were pure (a good approximation due to their very low mutual solubility), the enthalpy of dissociation of the clathrate ΔH_d could be written in terms of the enthalpy of melting of the corresponding empty clathrate frame, ΔH_m^{empty}, the enthalpy of methane with respect to a state without intermolecular interactions, $\Delta H_{methane}^{\infty}$, and the enthalpy for enclathrating the methane from a noninteracting gas state into the water clathrate frame, $\Delta H_{methane-water}^{enclathration}$:

$$\Delta H_d = 5.75\Delta H_m^{empty} - \Delta H_{methane}^{\infty} - \Delta H_{methane-water}^{enclathration} \quad (3)$$

where 5.75 is the ratio of water to methane in a fully occupied sI clathrate. The experimental enthalpy of dissociation of sI methane hydrate at 100 atm is $\Delta H_d = 13.01$ kcal per mol of gas.[45] In ref 7 we computed $\Delta H_m^{empty} = 1.05$ kcal/mol at 250 K, resulting in $5.75\Delta H_m^{empty} \approx 6.04$ kcal/mol (and expected to be larger at 300 K because the heat capacity of the liquid is larger than the heat capacity of the crystal). $\Delta H_{methane}^{\infty}$ is 0.82 kcal/mol for the M_{SW} model at 300 K and 100 atm (Table 3). This indicates that about half the enthalpy of dissociation of methane hydrate originates in the interaction between water and methane in the crystal.

As the average hydration number for methane in the fully occupied sI clathrates is 23 and the maximum water−methane interaction is ε_{wm}, to reproduce the experimental enthalpy of dissociation the value of ε_{wm} should be around 0.3 kcal/mol. We evaluated ΔH_d, of the sI clathrate at 100 atm for combinations of [σ_{wm}; ε_{wm}]. The results are listed in Table 4. ΔH_d was determined by subtracting the enthalpy of the clathrate phase from that of the separated methane and liquid water phases, each of them weighted by the stoichiometry of the reaction of formation of the sI clathrate. The enthalpies of methane and liquid water were determined from separate simulations of the coarse-grained M_{SW} and mW models at 300 K and 100 atm.

Table 4 shows that $\varepsilon_{wm} \approx 0.30$ kcal/mol overestimates the melting temperature by about 45 K. The mismatch indicates a lower entropy of dissociation of the coarse-grained model compared to that of the experiment. The enthalpy of dissociation of the clathrate ΔH_d and its corresponding phase equilibrium temperature T_m are related through $T_m = \Delta H_d/\Delta S_d$, where ΔS_d is the entropy of dissociation of the clathrate. The ΔS_d for the coarse-grained model should be lower than in the experiment because the mW water and M_{SW} methane do not have a rotational contribution to the entropy, and that should be significant for the fluids but not for the crystal phase. This limits the ability to simultaneously reproduce the T_m and the ΔH_d using a coarse-grained model. (The same should happen when atomistic models of water are combined with united atom models of methane such as the OPLS-UA model.) We note that all nonpolarizable atomistic models of water also underestimate the enthalpy of melting. For example, the T_m and ΔH_m of TIP4P/ice,[29] arguably the most accurate nonpolarizable atomistic model of water, are 272.2 K and 1.29 kcal/mol, essentially the same as for the monatomic water model mW, 274 K and 1.26 kcal/mol. For pure water, mW reproduces the experimental melting temperature of ice, while it underestimates the enthalpy of melting by 12% (1.436 kcal/mol in the experiment) and the entropy of melting by the same amount (4.61 in mW vs 5.26 cal/kmol in experiment).[33] A larger underestimation for clathrates than for ice melting is expected because of the additional contribution of the rotational entropy of methane.

Table 4 lists the enthalpy and entropy of dissociation of the sI clathrate for different water−methane potentials. The entropies of dissociation of all water−methane potentials in the coarse-grained simulations are about the same, $\Delta S_d \sim 34$ cal/kmol. This is ~75% of the experimental value, and a potential that reproduces T_m should underestimate ΔH_d by the same amount. Increasing the water−methane interaction parameter ε_{wm} leads to better agreement in ΔH_d at the expense of a worse prediction of the melting temperature. In conclusion, it is not possible to reproduce simultaneously the dissociation enthalpy and melting temperature; we privilege the latter in the parametrization of the water−methane potential because there is a physical reason for a lower entropy of melting in the coarse-grained model. In the next section we show that an increase in the water−methane attraction to produce better agreement for ΔH_d not only degrades the agreement in T_m but also leads to a high solubility of the "methane" it purportedly models.

V. Structure and Thermodynamics of Water−Methane Solutions

A. Solubility of Methane in Liquid Water. The solubility of methane in water was computed from large-scale simulations of water−methane systems in which the aqueous and organic

phases coexist in equilibrium (lower panel of Figure 1). The simulations were performed at $p = 178$ atm and $T = 313$ K to compare with the experimental solubility determined by Chapoy et al., $x_m = 0.002325$ methane molar fraction.[48] The solubility of methane in liquid water was evaluated for the same set of $[\sigma_{wm}; \varepsilon_{wm}]$ used for the analysis of the thermodynamics of the clathrates.

The solubility was computed as the average molar fraction of methane in the bulk of the water phase, determined from the water and methane density profiles along the direction perpendicular to the water−methane interfaces (see Figure 1c). The solubilities for the candidate water−methane potentials decrease, as expected, with the strength of the water−methane interaction, spanning from the experimental value to an order of magnitude higher (Table 4) The water−methane parameters $\sigma_{wm} = 4.0$ Å and $\varepsilon_{wm} = 0.18$ kcal/mol reproduce the experimental solubility: 0.0022 ± 0.0001 compared to 0.002 325.[48] This is also the potential that best reproduces the T_m of the sI and sII crystals. In what follows, when we refer to results for methane and water in the simulations, we use the models with the parameters collected in Table 1.

To assess whether the curved interface present in the direct coexistence simulation cells (Figure 1) significantly affects the solubility, we evaluated x_m in an *NpT* simulation of a liquid system of 2944 water molecules and 512 methane molecules, corresponding to the same composition of the liquid half of the beginning of the direct coexistence simulations for an sI clathrate, at 313 K and 178 atm. The liquid segregated to form a cylindrical region of methane fluid, as seen in the two upper panels of Figure 1. Using a clustering algorithm to determine the number of methane molecules that did not belong to the methane cylinder phase, we computed the molar fraction of dissolved methane in equilibrium. We averaged the molar fraction of methane solute in the water phase over 145 ns simulations. The result, 0.0025 ± 0.0008, compares very well with the 0.0022 ± 0.0001 determined from simulations with a flat interface.

B. Diffusion Coefficients. Molecular diffusion is faster in the coarse-grained models, due to the lack of explicit hydrogen atoms.[33] At 298 K and 1 atm, the diffusion coefficient in mW water is 2.8 times larger than in experiments, 6.5×10^{-5} cm^2/s vs 2.3×10^{-5} cm^2/s.[33,43] We computed the self-diffusion coefficient D of methane in water under the same conditions from the mean square displacement using Einstein's relation:

$$6Dt = \lim_{t\to\infty}\langle|\mathbf{r}_i(t) - \mathbf{r}_i(0)|^2\rangle \quad (4)$$

The coarse-grained model predicts a self-diffusion coefficient of methane in water $D = 4.8 \times 10^{-5}$ cm^2/s. This is 2.6 times the experimental result, 1.84×10^{-5} cm^2/s at 298 K.[49] This indicates that although the coarse-grained model overestimates the actual values of D, it faithfully represents the relative mobilities of the two components. This is not unexpected, as methane diffusion is probably enslaved to the mobility of the water solvent.

C. Methane Hydration in Solution. The experimental average coordination number of methane in the sI hydrate clathrates is 21 ± 1.[50] The average hydration in the crystal results from an average over the occupancy of the dodecahedral and hexakaidecahedral cages that contain 20 and 24 water molecules, respectively. In liquid water, the hydration number of methane has been determined to be 19 ± 1 by integration of the first peak of the oxygen−carbon radial distribution function (rdf or $g(r)$) obtained from neutron diffraction[51] and 20 by analysis of the chemical shifts of ^{13}C through NMR.[52] We computed the hydration number of methane in solution from the integration of the first peak of the rdf between water and methane at 100 atm and 300 K. The rdf for each of the candidate water−methane interaction potentials was averaged over 100 ns equilibrium simulation. We find that the water−methane $g(r)$ is not especially sensitive to the water−methane interaction within the parameter space we sampled: Figure 3 shows that water−methane interactions that produce a broad range of solubilities and melting temperatures yield similar water−methane $g(r)$. The experimental position of the first peak ($r_{max} = 3.5$ Å) and first minimum (r_{min} between 5.0 and 5.2 Å) are well reproduced by the simulations (e.g., 3.5 and 5.22 Å, respectively, for $\sigma_{wm} = 4.0$ Å and $\varepsilon_{wm} = 0.18$ Å. We computed the hydration number n_w by integration of the first peak of the water−methane $g(r)$,

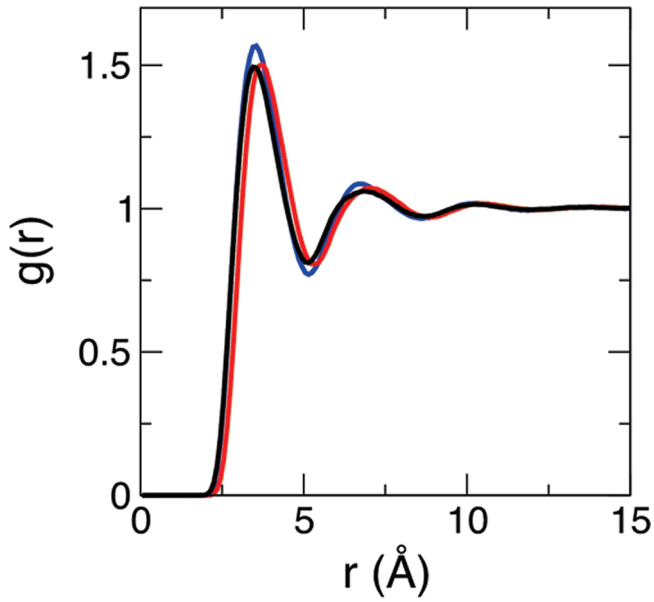

Figure 3. Water−methane radial distribution function $g(r)$ for three different sets of water−methane interaction parameters, $[\sigma_{wm}; \varepsilon_{wm}]$: [4.0 Å; 0.18 kcal/mol] in black; [4.05 Å; 0.24 kcal/mol] in red; [3.75 Å; 0.25 kcal/mol] in blue. While these parameters produce greatly different solubilities and melting temperatures (see Table 4), they all yield fairly similar water−methane distribution functions and hydration numbers.

$$n_w = 4\pi\rho_w \int_0^{r_{min}} r^2 g(r)\, dr \quad (5)$$

where ρ_w is number density of water. n_w values for the different water−methane parameters are listed in Table 4. The hydration number ranges from 18.9 to 21.8, increasing with the size σ_{wm} and strength σ_{wm} of the water−methane potential. The parameters summarized in Table 1, which best reproduce the T_m and ΔT_m of methane clathrates and the solubility of methane in water, predict a hydration number of 19.3, in very good agreement with the 20 and 19 ± 1 deduced from the experiments.[51,52]

D. Surface Tension of the Water−Methane Interface. We calculated the surface tension of the water−methane interface from a 100 ns *NVT* simulation of the system in Figure 1c. The surface tension was determined using the relation[53]

$$\gamma = \frac{L_z}{2}[\langle p_N \rangle - \langle p_T \rangle] \quad (6)$$

where $L_z = 230$ Å is the length of the simulation cell perpendicular to the methane−water interface and $\langle p_N \rangle$ and $\langle p_T \rangle$ are the time-averaged components of the pressure tensors perpendicular and tangential to the methane−water interface, respectively. The coarse-grained model predicts a methane−water surface tension of 57 mN/m at 300 K and 100 atm compared to the experimental result of 61 mN/m under the same conditions.[54] The level of agreement is comparable to that previously reported for the surface tension of the liquid water−vacuum interface at 298 K: 66 mN/m for mW vs 71.6 mN/m in experiment.[33] The similarity in surface tension between water−vacuum and water−methane is consistent with the high hydrophobicity of methane.

E. Width of the Methane−Water Interface. The solubility of methane in liquid water is 2 orders of magnitude lower than in the hydrate crystals. Experiments indicate that nucleation of clathrates occurs close to or at the water−methane interface, where methane availability is the highest.[31] It is not clear, however, whether the nucleation occurs at the interface itself or in its immediacy, and this may be controlled by the width of the interface, which determines what is the spatial range over which the concentration of methane in water is comparable to that found in the methane hydrate.

Reed and Westacott used the SPC/E water model and the OPLS-UA methane model to determine the t_{90-10} width of the interface (the width over which the density of each component decays from 90% to 10% of the bulk density).[55] They found a t_{90-10} for water of 3.19 Å at 280 K and 120 atm. We computed the methane and water density profiles from the two-phase simulations at $T = 313$ K and $p = 178$ atm we used for the determination of the solubility. The width of the interface was rather insensitive to the change of the parameters of the water−methane potential used in this study. The methane and water density profiles for the model with the parameters of Table 1 are shown in Figure 4. The t_{90-10} length for the coarse-grained system is 4.0 Å. We note that both the atomistic and coarse-grained models predict that the width of the region for which the local concentration of methane is comparable to that in the clathrate is about the diameter of a water molecule. This is much narrower than the smallest clathrate cage, a water dodecahedron.

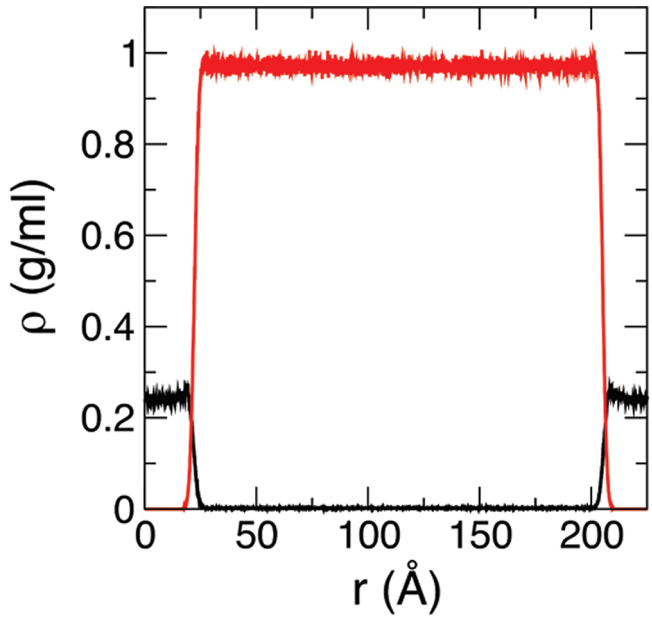

Figure 4. Density profile of water (red) and methane (black) in a two-phase liquid system (see Figure 1c) at $T = 313$ K and $p = 178$ atm. Interactions modeled with the parameters of Table 1. The width of the interface (4 Å) is narrower than a complete dodecahedral clathrate cage.

VI. Conclusion

In this work we developed a coarse-grained model for molecular simulations of water and methane. The methane and water molecules were represented as single particles interacting through short-ranged potentials. Water was modeled with the monatomic model of water mW that uses a combination of two- and three-body interactions to reproduce the anisotropic, hydrogen-bonded structures that water forms in its liquid, amorphous solid, ice, and clathrate phases.[7,33−35] Methane−methane interactions were described by short-ranged pair potentials parametrized to reproduce the enthalpy of vaporization and density of liquid methane at the experimental normal boiling point. We find that our united atom methane model is less transferable across a broad range of pressures than the OPLS-UA methane based on a Lennard-Jones potential, a difference that we attribute to the softness of the pair potential in the present study. While clathrate forming conditions usually involve high pressures, in the order of tens to hundreds of atmospheres,[2] we did not further refine the methane model because the error in the enthalpy of methane at 100 atm is about 2% of the enthalpy of formation of methane hydrate.

The parametrization of the water−methane interactions was the main focus of this study. The search for the optimum size σ_{wm} and strength ε_{wm} that define the water−methane potential was conducted in a reduced region of the parameter space where the sI hydrate with methane occupying the small and large water cages, experimentally the most stable crystal form of methane hydrate, has a lower enthalpy of formation than other clathrate structures. Properties that are key for the thermodynamics and structure of aqueous methane solutions and the formation and stability of methane clathrates were used for the parametrization and validation of the water−methane interactions: the solubility and hydration number of methane in liquid water, the surface tension and width of the water−methane interface, the enthalpy of dissociation of the sI methane hydrate crystal, and the temperature of melting of the stable (sI) and metastable (sII) methane hydrate polymorphs. The parameters that best reproduce these properties are listed in Table 1. Below we discuss the significance of each of these properties and the level of agreement between the coarse-grained model and experiment.

At a fundamental level, the solubility of methane is a measure of its excess chemical potential in water. From the point of view of the modeling of clathrate nucleation and growth, the low solubility of methane provides a barrier for the formation of clathrates that could control the determining step for the rate of crystallization.[56] Under the conditions of this study, 178 atm and 313 K, the solubilities of the coarse-grained model and experiment are identical, 0.0022 ± 0.0001 and 0.002325,[48] respectively. An analysis of the temperature and pressure dependence of the solubility exceeds the scope of this study and is left for future work. Nevertheless, we note here that there is a correlation between the ability of a water model in reproducing the temperature dependence of the solubility of small hydrophobic molecules and the temperature evolution of the density.[27] The mW model correctly predicts the density of water around room temperature and, at lower temperatures,

the existence of a density maximum followed by a sharp decrease in the density of liquid water that precedes its transformation into low-density amorphous ice.[33] This strongly suggests that this coarse-grained model would reproduce the increasing solubility on cooling that is a characteristic of hydrophobic hydration.[57−59]

The formation of clathrate crystals from aqueous solutions involves diffusion of water and methane and reorganization of the water structure around the methane to form the polyhedral water cages characteristic of each crystal phase. The coarse-grained model overestimates the mobility of water and methane in solution by a factor of about 2.7 but correctly describes the ratio between the diffusivity of water and methane. An accurate representation of the hydration shell of methane in water is a necessary (although probably not sufficient[60]) condition for the correct modeling of the nucleation of clathrates. The hydration number of methane in water predicted by the coarse-grained model, 19.3, is in very good agreement with that determined from NMR,[52] $n_w = 20$, and neutron diffraction,[51] $n_w = 19 \pm 1$. As a further characterization of the hydration shell, we compared the water−methane radial distribution functions for dilute methane in water with that obtained from the neutron diffraction experiments and found good agreement for the positions of the first maximum and minimum of the rdf.

The melting temperature of the clathrates is central for the determination of their regions of stability and the driving force for crystallization under nonequilibrium conditions. Although sI is the stable structure of methane hydrates, sII crystals also form in the initial stages of crystallization.[9,10] The melting temperatures of these two structures are close, just 1.5 K apart at 100 atm according to our calculations with the CSM-Gem program. Reproducing the melting temperatures of sI and sII and their small stability gap is crucial for the study of the origin of the mechanism of cross-nucleation in clathrates. Nevertheless, determinations of the melting temperature of methane hydrates with atomistic models have been scarce for the sI structure and nonexistent for the sII crystal. The coarse-grained model developed in this study predicts a melting temperature of 285 ± 4 K for the sI hydrate and 286 ± 1 for the sII crystal, in excellent agreement with 286.2 and 284.2, respectively, predicted by experiment and the CSM-Gem program. We have shown that the lack of rotational degrees of freedom in the monatomic water and methane leads to an underestimation of the entropy of melting by about 25%, which (combined with an accurate description of melting temperature) leads to an equivalent underestimation of the enthalpy of dissociation of the clathrate. Other models that approximate methane by a single particle (e.g., the OPLS-UA model) would face the same intrinsic limitation, although less pronounced while combined with atomistic models of water.

Finally, we have evaluated the surface tension and width of the water−methane interface, which could be a locus of crystallization of methane hydrate. The coarse-grained model reproduces the water−methane and water−vacuum surface tensions within 7% of the experiment. In the absence of experimental data on the width of the interface, we compared the coarse-grained results with those of a recent atomistic study using SPC/E water with OPLS-UA methane. The two simulations predict that the water−methane interface is sharp, its width about the diameter of a water molecule. This indicates that the region for which the average concentration of methane in the liquid is comparable to the concentration in the methane clathrate, local conditions that would favor crystallization, is narrower than the size of the smaller clathrate cage.

We are not aware of any other coarse-grained molecular model for water and methane that is parametrized to reproduce actual experimental properties of their liquid and crystal phases. We expect that this coarse-grained model will be instrumental in the study of the mechanisms of nucleation and growth of methane clathrates under various thermodynamic conditions with knowledge of the crystallization driving force. Water interaction with hydrophobic moieties plays a pivotal role in determining the structure and function of biomolecules and assembly of nanoparticles: hydrophobic forces drive the self-assembly of micelles and lipid bilayers,[61] protein structure is heavily influenced by hydrophobic interactions[62] and the subtle influence of the hydrophobic effect limits the conditions at which the correctly folded protein structures retain their functionality before they denature at high and low temperature as well as elevated pressure,[63] and hydrophobic interactions shape the structure of DNA and the interaction of its complexes.[64] Coarse-grained modeling of these complex structures requires an accurate model of water and its interactions with hydrophobic, hydrophilic, and ionic groups. Previously, the mW model has been extended for the modeling of electrolytes in solution, without the use of electrostatics or other long-ranged interactions.[43] We expect that the methane−water model of this work will be useful for the study of hydrophobic assembly in aqueous solutions and provide a stepping-stone for the parametrization of coarse-grained models of organic and biological molecules with explicit solvation.

Acknowledgment. This work has been supported by the Beckman Foundation through a Young Investigator Award to V.M. and by the National Science Foundation through Collaborative Research grant CHE-0628257. We acknowledge the Center of High Performance Computing at the University of Utah for allocation of computing time.

References and Notes

(1) Sloan, E. D. *Nature* **2003**, *426*, 353.
(2) Sloan, E. D.; Koh, C. A. *Clathrate Hydrates of Natural Gases*, 3rd ed.; CRC Press/Taylor-Francis: Boca Raton, FL, 2007.
(3) Koh, C. A.; Sum, A. K.; Sloan, E. D. *J. Appl. Phys.* **2009**, *106*, 061101.
(4) Brewer, P. G.; Friederich, C.; Peltzer, E. T.; Orr, F. M. *Science* **1999**, *284*, 943.
(5) Park, Y.; Kim, D.-Y.; Lee, J.-W.; Huh, D.-G.; Park, K.-P.; Lee, J.; Lee, H. *Proc. Natl. Acad. Sci. U.S.A.* **2006**, *103*, 12690.
(6) Koh, C. A. *Chem. Soc. Rev.* **2002**, *31*, 157.
(7) Jacobson, L. C.; Hujo, W.; Molinero, V. *J. Phys. Chem. B* **2009**, *113*, 10298.
(8) Conde, M. M.; Vega, C.; Tribello, G. A.; Slater, B. *J. Chem. Phys.* **2009**, *131*, 034510.
(9) Schicks, J. M.; Ripmeester, J. A. *Angew. Chem., Int. Ed.* **2004**, *43*, 3310.
(10) Choukroun, M.; Morizet, Y.; Grasset, O. *J. Raman Spectrosc.* **2007**, *38*, 440.
(11) Ballard, L.; Sloan, E. D. *Fluid Phase Equilib.* **2004**, *216*, 257.
(12) Walsh, M. R.; Koh, C. A.; Sloan, E. D.; Sum, A. K.; Wu, D. T. *Science* **2009**, *326*, 1095.
(13) Jacobson, L. C.; Hujo, W.; Molinero, V. Initial Pathways in the Nucleation of Clathrate Hydrates: Effect of Guest Size and Hydrophilicity. Manuscript in preparation.
(14) Susilo, R.; Alavi, S.; Ripmeester, J.; Englezos, P. *Fluid Phase Equilib.* **2008**, *263*, 6.
(15) Alavi, S.; Ripmeester, J. A.; Klug, D. D. *J. Chem. Phys.* **2007**, *126*, 124708.
(16) Vatamanu, J.; Kusalik, P. G. *J. Phys. Chem. B* **2008**, *112*, 2399.
(17) Anderson, B. J.; Tester, J. W.; Borghi, G. P.; Trout, B. L. *J. Am. Chem. Soc.* **2005**, *127*, 17852.
(18) Ding, L. Y.; Geng, C. Y.; Zhao, Y. H.; Wen, H. *Mol. Simul.* **2007**, *33*, 1005.
(19) English, N. J.; Johnson, J. K.; Taylor, C. E. *J. Chem. Phys.* **2005**, *123*, 244503.

(20) Jiang, H.; Myshakin, E. M.; Jordan, K. D.; Warzinski, R. P. *J. Phys. Chem. B* **2008**, *112*, 10207.
(21) English, N. J.; Tse, J. S.; Carey, D. J. *Phys. Rev. B* **2009**, *80*, 134306.
(22) Hawtin, R. W.; Quigley, D.; Rodger, P. M. *Phys. Chem. Chem. Phys.* **2008**, *10*, 4853.
(23) Asthagiri, D.; Merchant, S.; Pratt, L. R. *J. Chem. Phys.* **2008**, *128*, 244512.
(24) Czaplewski, C.; Rodziewicz-Motowidlo, S.; Liwo, A.; Ripoll, D. R.; Wawak, R. J.; Scheraga, H. A. *Protein Sci.* **2000**, *9*, 1235.
(25) Docherty, H.; Galindo, A.; Vega, C.; Sanz, E. *J. Chem. Phys.* **2006**, *125*, 074510.
(26) Konrad, O.; Lankau, T. *J. Phys. Chem. B* **2005**, *109*, 23596.
(27) Paschek, D. *J. Chem. Phys.* **2004**, *120*, 6674.
(28) Sobolewski, E.; Makowski, M.; Oldziej, S.; Czaplewski, C.; Liwo, A.; Scheraga, H. A. *Protein Eng. Des. Sel.* **2009**, *22*, 547.
(29) Abascal, J. L. F.; Sanz, E.; Fernandez, R. G.; Vega, C. *J. Chem. Phys.* **2005**, *122*, 234511.
(30) Vega, C.; Sanz, E.; Abascal, J. L. F. *J. Chem. Phys.* **2005**, *122*, 114507.
(31) Mastny, E. A.; Miller, C. A.; de Pablo, J. J. *J. Chem. Phys.* **2008**, *129*, 034701.
(32) Myshakin, E. M.; Jiang, H.; Warzinski, R. P.; Jordan, K. D. *J. Phys. Chem. A* **2009**, *113*, 1913.
(33) Molinero, V.; Moore, E. B. *J. Phys. Chem. B* **2009**, *113*, 4008.
(34) Moore, E. B.; de la Llave, E.; Welke, K.; Scherlis, D. A.; Molinero, V. *Phys. Chem. Chem. Phys.* **2010**, *12*, 4124.
(35) Moore, E. B.; Molinero, V. Ice Crystallization in Water's "No-Man's Land". *J. Chem. Phys.*, in review.
(36) Moore, E. B.; Molinero, V. *J. Chem. Phys.* **2009**, *130*, 244505.
(37) Jacobson, L. C.; Molinero, V. Nucleation and growth of clathrate hydrates with a coarse-grained water model. In *237th ACS National Meeting & Exposition, Gas Hydrates and Clathrates Symposium*, Salt Lake City, 2009.
(38) Plimpton, S. J. *J. Comput. Phys.* **1995**, *117*, 1.
(39) Stillinger, F. H.; Weber, T. A. *Phys. Rev. B* **1985**, *31*, 5262.
(40) Jorgensen, W. L.; Madura, J. D.; Swenson, C. J. *J. Am. Chem. Soc.* **1984**, *106*, 6638.
(41) Martin, M. G.; Siepmann, J. I. *J. Phys. Chem. B* **1998**, *102*, 2569.
(42) Chen, B.; Siepmann, J. I. *J. Phys. Chem. B* **1999**, *103*, 5370.
(43) DeMille, R. C.; Molinero, V. *J. Chem. Phys.* **2009**, *131*, 034107.
(44) Setzmann, U.; Wagner, W. *J. Phys. Chem. Ref. Data* **1991**, *20*, 1061.
(45) Gupta, A.; Lachance, J.; Sloan, E. D., Jr.; Koh, C. A. *Chem. Eng. Sci.* **2008**, *63*, 5848.
(46) Yoo, S.; Zeng, X. C.; Morris, J. R. *J. Chem. Phys.* **2004**, *120*, 1654.
(47) Fernandez, R. G.; Abascal, J. L. F.; Vega, C. *J. Chem. Phys.* **2006**, *124*, 144506.
(48) Chapoy, A.; Mohammadi, A. H.; Richon, D.; Tohidi, B. *Fluid Phase Equilib.* **2004**, *220*, 111.
(49) Jähne, B.; Heinz, G.; Dietrich, W. *J. Geophys. Res.* **1987**, *92*, 10767.
(50) Koh, C. A.; Wisbey, R. P.; Wu, X. P.; Westacott, R. E.; Soper, A. K. *J. Chem. Phys.* **2000**, *113*, 6390.
(51) De Jong, P. H. K.; Wilson, J. E.; Neilson, G. W.; Buckingham, A. D. *Mol. Phys.* **1997**, *91*, 99.
(52) Dec, S. F.; Bowler, K. E.; Stadterman, L. L.; Koh, C. A.; Sloan, E. D. *J. Am. Chem. Soc.* **2005**, *128*, 414.
(53) Gloor, G. J.; Jackson, G.; Blas, F. J.; de Miguel, E. *J. Chem. Phys.* **2005**, *123*, 134703.
(54) Sachs, W.; Meyn, V. *Colloids Surf., A* **1995**, *94*, 291.
(55) Reed, S. K.; Westacott, R. E. *Phys. Chem. Chem. Phys.* **2008**, *10*, 4614.
(56) Radhakrishnan, R.; Trout, B. L. *J. Chem. Phys.* **2002**, *117*, 1786.
(57) Chandler, D. *Nature* **2005**, *437*, 640.
(58) Southall, N. T.; Dill, K. A.; Haymet, A. D. J. *J. Phys. Chem. B* **2001**, *106*, 521.
(59) Pratt, L. R.; Pohorille, A. *Chem. Rev.* **2002**, *102*, 2671.
(60) Guo, G. J.; Zhang, Y. G.; Li, M.; Wu, C. H. *J. Chem. Phys.* **2008**, *128*, 194504.
(61) Tanford, C. *Science* **1978**, *200*, 1012.
(62) Raschke, T. M. *Curr. Opin. Struct. Biol.* **2006**, *16*, 152.
(63) Pratt, L. R. *Annu. Rev. Phys. Chem.* **2003**, *53*, 409.
(64) von Hippel, P. H. *Annu. Rev. Biophys. Biomol. Struct.* **2007**, *36*, 79.

JP1013576